OPEN ACCESS
CellPress

Cell Reports
Article

Cdk1 Coordinates Timely Activation of MKlp2 Kinesin with Relocation of the Chromosome Passenger Complex for Cytokinesis

Mayumi Kitagawa,[1,4] Suet Yin Sarah Fung,[1,4] Umar Farook Shahul Hameed,[2] Hidemasa Goto,[3] Masaki Inagaki,[3] and Sang Hyun Lee[1,*]

[1]Program in Cancer and Stem Cell Biology, Duke-NUS Graduate Medical School, 8 College Road, Singapore 169857, Singapore
[2]Department of Biological Sciences, National University of Singapore, Singapore 117543, Singapore
[3]Division of Biochemistry, Aichi Cancer Center Research Institute, Nagoya, Aichi 464-8681, Japan
[4]Co-first authors
*Correspondence: sanghyun.lee@duke-nus.edu.sg
http://dx.doi.org/10.1016/j.celrep.2014.02.034

SUMMARY

The chromosome passenger complex (CPC) must relocate from anaphase chromosomes to the cell equator for successful cytokinesis. Although this landmark event requires the mitotic kinesin MKlp2, the spatiotemporal mechanistic basis remains elusive. Here, we show that phosphoregulation of MKlp2 by the mitotic kinase Cdk1/cyclin B1 coordinates proper mitotic transition with CPC relocation. We identified multiple Cdk1/cyclin B1 phosphorylation sites within the stalk and C-terminal tail that inhibit microtubule binding and bundling, oligomerization/clustering, and chromosome targeting of MKlp2. Specifically, inhibition of these abilities by Cdk1/cyclin B1 phosphorylation is essential for proper early mitotic progression. Upon anaphase onset, however, reversal of Cdk1/cyclin B1 phosphorylation promotes MKlp2-CPC complex formation and relocates the CPC from anaphase chromosomes for successful cytokinesis. Thus, we propose that phosphoregulation of MKlp2 by Cdk1/cyclin B1 ensures that activation of MKlp2 kinesin and relocation of the CPC occur at the appropriate time and space for proper mitotic progression and genomic stability.

INTRODUCTION

For successful cell division, faithful segregation of duplicated sister chromatids to two daughter cells must be orchestrated with cytokinesis. A key component coordinating this process is the chromosome passenger complex (CPC), which consists of the enzymatic component Aurora B and three regulatory components: INCENP, survivin, and borealin (reviewed by Carmena et al., 2012). The CPC is essential for proper chromosome congression in early mitosis at the centromeres, while it relocates to the spindle midzone and equatorial cortex (hereby called the cell equator) in late mitosis (Cooke et al., 1987; Earnshaw and Cooke, 1991) to promote furrow ingression for cytokinesis.

The CPC relocation event starts at the metaphase-to-anaphase transition, a point of no return that is tightly regulated by maintaining Cdk1/cyclin B1 kinase activity (reviewed by Rhind and Russell, 2012). For this transition to occur, bipolar spindle attachment must be completed in order for the anaphase-promoting complex (APC) to degrade cyclin B1 that inactivates Cdk1. In budding yeast, Cdk1 and Cdc14p phosphatase antagonistically control Sli15/INCENP for Ipl1/Aurora B localization (Mirchenko and Uhlmann, 2010; Nakajima et al., 2011; Pereira and Schiebel, 2003). In mammalian cells, Cdk1/cyclin B1 phosphorylation of INCENP at the Thr-59 residue has an inhibitory effect on CPC relocation (Goto et al., 2006; Hümmer and Mayer, 2009). However, the mechanistic basis of the spatiotemporal redistribution of the CPC upon anaphase onset remains elusive, particularly in mammalian cells. Furthermore, despite the requirement of MKlp2 kinesin for CPC relocation and cytokinesis in mammalian cells (Gruneberg et al., 2004; Hill et al., 2000), the mechanism of spatiotemporal recognition between MKlp2 and the CPC at anaphase onset is unclear.

Here, we show a key regulatory mechanism that controls activation of MKlp2 at the appropriate time in the cell cycle via Cdk1/cyclin B1-mediated phosphoregulation. In brief, we demonstrate that Cdk1/cyclin B1-mediated inhibitory phosphorylation of MKlp2 is essential for proper early mitotic progression. Upon anaphase onset, however, reversing this phosphorylation is necessary for timely activation of MKlp2 kinesin to relocate the CPC from anaphase chromosomes for cytokinesis. Thus, Cdk1/cyclin B1-mediated phosphoregulation ensures that activation of MKlp2 kinesin and relocation of the CPC occur at the appropriate time and space for proper mitotic progression.

RESULTS

Cdk1/Cyclin B1-Dependent Phosphorylation of MKlp2 in Early Mitosis

It is unclear how MKlp2 kinesin function is controlled during mitotic progression. Notably, when HeLa cells arrested in mitosis

by the microtubule depolymerizer nocodazole (Noco) were briefly treated with the Cdk1 inhibitor purvalanol A (PurvA), endogenous MKlp2 showed band-shifting into a form of higher mobility in Phos-tag SDS-PAGE (Figure 1A), suggesting dephosphorylation. To evaluate the possibility of phosphoregulation of MKlp2, HeLa cell lines engineered to express Flag-tagged MKlp2 (Flag-MKlp2) at endogenous levels upon doxycycline (Dox) treatment (Kitagawa et al., 2013) were synchronized in prometaphase-like state by Noco treatment. After release, cells were harvested at different time points. Phos-tag SDS-PAGE revealed the mitotic mobility shift of the Flag-MKlp2^{WT} band gradually collapsing at anaphase onset (marked by a decrease in cyclin B1 levels) (Figure 1B). Although the amount of extracted Flag-MKlp2^{WT} also decreased after anaphase onset (Figure 1B, lanes 3 and 4), it was mainly due to Flag-MKlp2^{WT} becoming less soluble (Figures 2E, 2F, and 4C). Moreover, treating immunopurified Flag-MKlp2^{WT} with alkaline phosphatase (ALP) also caused band-shifting (Figure 1C, lanes 3 and 4), suggesting that MKlp2 is phosphorylated in early mitosis.

Human MKlp2 contains seven putative, evolutionarily conserved proline-directed Cdk1 phosphorylation sites (Figure 1D; Figure S1A). Indeed, Cdk1/cyclin B1 phosphorylated multiple proline-directed Ser/Thr residues in MKlp2 in vitro (Figure S1B). Thus, to determine whether the band-shifting of Flag-MKlp2^{WT} was due to phosphorylation of these residues, we substituted all putative phosphoresidues with alanine (MKlp2^{7A}; Figure 1D). Indeed, Flag-MKlp2^{7A} did not show a measurable band-shifting unlike Flag-MKlp2^{WT} (Figure 1E, lanes 2 and 4), even after ALP treatment (Figure 1C, lanes 7 and 8), suggesting that MKlp2 is phosphorylated on all or some proline-directed Ser/Thr residues. Thus, we conclude that MKlp2 is phosphorylated in early mitosis (at least in mitotic-arrested cells with spindle damages) in a Cdk1/cyclin B1-dependent manner.

Cdk1/Cyclin B1 Restrains MKlp2 in the Cytoplasm in Early Mitosis

Next, whether Cdk1/cyclin B1-dependent phosphorylation controls MKlp2 localization was tested. Notably, while endogenous MKlp2 localized in the cytoplasm of metaphase-arrested HeLa cells by the proteasome inhibitor MG132, a brief PurvA treatment for 2 min caused a dramatic redistribution of MKlp2 to the metaphase spindles, chromosomes, and the cell cortex without apparent chromosome separation (Figure 1F). Furthermore, in metaphase-arrested HeLa cells, Dox-induced Flag-MKlp2^{7A}, but not Flag-MKlp2^{WT}, constitutively localized to the metaphase spindles, chromosomes, and the cell cortex and induced misaligned chromosomes (Figure 1G, arrows; see also Figure 3H). Consistent with this localization pattern of MKlp2 determined by immunofluorescence staining, transiently expressed mCherry-tagged MKlp2^{7A}, but not MKlp2^{WT}, showed a similar localization pattern in HeLa cells arrested by inhibiting centrosome separation with the Eg5 inhibitor S-trityl-L-cysteine (STLC) (Figure 1H, subpanels a and b; Figure 1I). Thus, we conclude that Cdk1/cyclin B1 restrains MKlp2 in the cytoplasm in early mitosis.

Notably, alanine substitutions at the Ser-532, Thr-857, Ser-867, and Ser-878 residues (MKlp2$^{C\text{-}4A}$) in the stalk and C-terminal tail domains were sufficient to induce MKlp2 redistribution (Figure 1H, subpanel c; Figure 1I), although slightly weaker than MKlp2^{7A} (Figures 3C, 3D, 5G, and 5H). In contrast, alanine substitutions at the Ser-7 and Ser-21 residues in the N-terminal tail (MKlp2$^{N\text{-}2A}$) weakly caused MKlp2 redistribution to chromosomes (Figure 1I). Alanine substitution at the Thr-198 residue did not cause measurable changes (M.K. and S.H.L. unpublished data). Furthermore, none of phosphomimetic mutants (generated by glutamate substitution) showed any measurable redistribution (Figure 1I). Interestingly, phosphoproteomic analysis (http://www.phosphosite.org) indicates that these 4 residues in the stalk and C-terminal tail domains are frequently phosphorylated. To determine the phosphorylation status of these residues in vivo, phosphospecific (pS-532, pS-867, and pS-878) antibodies were generated and validated for specificity (Figure S2). The phosphorylation status of the Thr-857 residue was determined by antibodies against a phospho-Thr-Pro motif (p-TP). Indeed, all phosphospecific antibodies strongly cross-reacted with Dox-induced Flag-MKlp2^{WT} in Noco-arrested HeLa cells, while PurvA treatment abolished such reactivity (Figure 1J, lanes 1 and 5). Notably, using these phosphospecific antibodies as indicators, these phosphoresidues were rapidly dephosphorylated upon anaphase onset (marked by a decrease in cyclin B1 levels) (Figure 1J). Thus, we conclude that Cdk1/cyclin B1 controls spatiotemporal localization of MKlp2 during mitotic progression via promoting phosphorylation of at least the stalk and C-terminal tail domains. This phosphorylation restrains MKlp2 in the cytoplasm in early mitosis.

Phosphoregulation of MKlp2 in Higher-Order Complex Formation, Direct Microtubule Binding, and Chromosome Targeting

Folding the tail and motor domains of kinesin together is a proposed mechanism for inhibiting kinesin motor (reviewed by Verhey and Hammond, 2009). Thus, whether C-terminal phosphorylation may maintain MKlp2 in a folded state was tested using recombinant MBP-tagged C-terminal tail (amino acids [aa] 710–890; MBP-MKlp2$^{710–890}$ and MBP-MKlp2$^{710–890/C\text{-}3E}$) and His-tagged N-terminal domain (aa 1–510; 6xHis-MKlp2$^{1–510}$) (Figure 2A). In contrast to our hypothesis, MBP-MKlp2$^{710–890}$ formed a complex with 6xHis-MKlp2$^{1–510}$ (Figure 2B, lanes 1–7) with patterns of sequential interaction (Figure 2C; K_D = 5.1 μM and K_D = 15.6 μM), while the phosphomimetic mutant MBP-MKlp2$^{710\text{-}890/C\text{-}3E}$ failed to do so in MBP-pull-down (Figure 2B, lanes 8–14) and isothermal titration calorimetry (ITC) assays (M.K. and S.H.L., unpublished data). Thus, Cdk1/cyclin B1-dependent phosphorylation may prevent the C-terminal tail from interacting with the motor domain.

Moreover, determined by sucrose density gradient centrifugation of cell lysates expressing mCherry-MKlp2, the majority of MKlp2^{WT} or the phosphoresistant MKlp2$^{C\text{-}4A}$ was found in the bottom fractions (Figure 2D). In contrast, the phosphomimetic MKlp2$^{C\text{-}4E}$ migrated much slower (Figure 2D), indicating that Cdk1/cyclin B1-dependent phosphorylation may inhibit higher-order complex formation (oligomerization/clustering or binding to large cellular components) of MKlp2. Previously characterized biochemical properties of the kinesin-6 family member MKlp1 becoming less soluble in low-ionic-strength solutions as well as during cytokinesis explains its tendency to assemble into

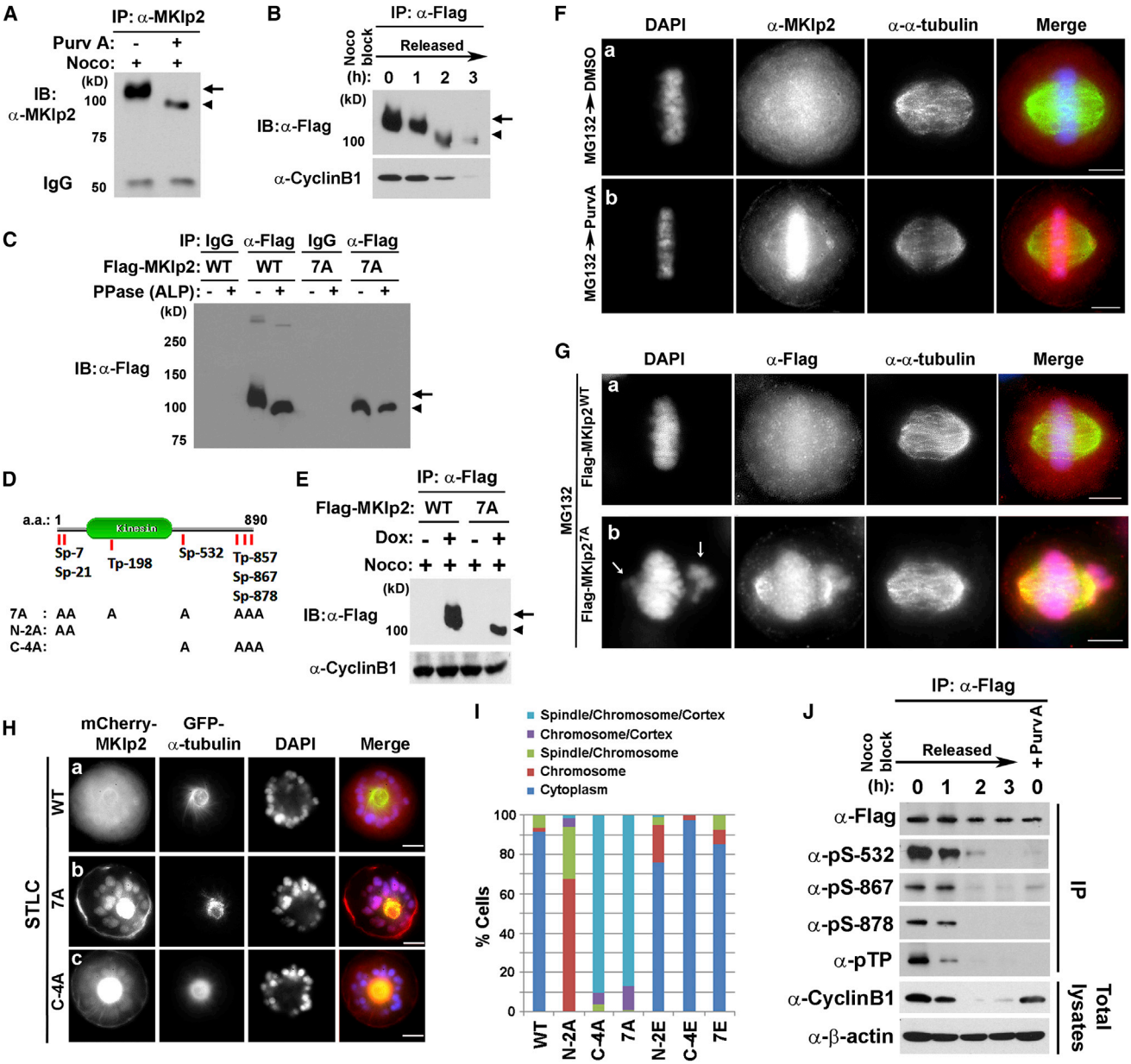

Figure 1. Cdk1/Cyclin B1-Dependent Phosphorylation Restrains MKlp2 in the Cytoplasm in Early Mitosis

(A–C and E) Phos-tag SDS-PAGE analysis of immunoprecipitated endogenous MKlp2 (A) or Flag-MKlp2 (B, C, and E). Noco-arrested HeLa cells were treated with PurvA (A) or synchronously released from Noco-block (B). Immunopurified Dox-induced Flag-MKlp2 was treated with ALP for 1 hr (C). Arrows indicate the slow-migrating hyperphosphorylated MKlp2, while arrowheads indicate the fast-migrating hypophosphorylated forms.

(D) Structural motifs of MKlp2 and putative proline-directed Ser (Sp)/Thr (Tp) phosphosites are shown (top). The list of phosphoresistant mutants used in this study is shown (bottom).

(F) HeLa cells were treated with MG132 (10 μM) for 1 hr and then with DMSO (subpanel a) or PurvA (subpanel b) before fixing in ice-cold methanol.

(G) Images of Dox-induced Flag-MKlp2 at metaphase. Dox-inducible HeLa cells were treated with Dox for 24 hr and MG132 for 1.5 hr before fixing in ice-cold methanol. Arrows indicate misaligned chromosomes (subpanel b).

(H and I) HeLa cells stably expressing GFP-α-tubulin were transfected with expression vectors encoding the indicated siRNA-resistant mCherry-MKlp2 together with MKlp2 siRNA for 6 hr. The cells were subsequently treated with STLC for 16 hr before fixing in ice-cold methanol. (I) The percentages of cells with an indicated pattern of mCherry-MKlp2 localization are shown (n > 100 cells per condition).

(J) Noco-arrested HeLa cells with Dox-induced Flag-MKlp2^{WT} were harvested at indicated times after synchronously released (lanes 1–4). Total cell lysates were subjected to immunoprecipitation using α-Flag antibodies followed by immunoblot analysis including indicated phosphospecific antibodies. For lane 5, Noco-arrested cells were treated with PurvA before harvesting.

White bars in (F)–(H) represent 5 μm.

motile clusters and stable accumulation at the spindle midzone (Hutterer et al., 2009; Mishima et al., 2002). Notably, when Noco-arrested HeLa cells were synchronously released, Flag-MKlp2^{WT} also became gradually less soluble as the levels of cyclin B1 declined (Figure 2E), indicating Cdk1/cyclin B1 phosphorylation may control solubility of MKlp2. Indeed, using pS-532 antibodies, only the dephosphorylated pool of MKlp2 preferentially became insoluble (Figure 2E). Furthermore, PurvA treatment to Noco-arrested HeLa cells induced Flag-MKlp2^{WT}, but not Flag-MKlp2$^{C\text{-}4E}$, insolubility (Figure 2F). Thus, we conclude that Cdk1/cyclin B1-dependent phosphorylation inhibits higher-order complex formation and promotes solubility of MKlp2 (possibly inhibiting oligomerization/clustering or interaction with large cellular components [e.g., microtubules, actin filaments, or chromosomes]).

Because the phosphoresistant mutant of MKlp2 prematurely localized to microtubules (Figures 1G–1I), instead of a folded-state model, we tested whether the C-terminal tail possesses a cryptic microtubule binding site. This idea was conceivable as an evolutionarily conserved stretch of basic residues (arrows) surrounds the phosphoresidues (asterisks) in this tail (Figure 2G). Indeed, in vitro microtubule cosedimentation analysis showed that MBP-MKlp2$^{710–890}$ directly bound microtubules, while the phosphomimetic MBP-MKlp2$^{710–890/C\text{-}3E}$ did so less efficiently (Figure 2H). This microtubule binding is charge dependent because increasing the salt concentration (potassium chloride [KCl]) decreased the microtubule binding of MBP-MKlp2$^{710–890}$ (Figure 2H, top panel), while a lower salt concentration abolished the microtubule binding of MBP-MKlp2$^{710\text{-}890/C\text{-}3E}$ (bottom panel). Thus, the Arg/Lys/His-rich basic clusters in the C-terminal tail directly mediate microtubule binding in a charge-dependent manner, whereas Cdk1/cyclin B1-dependent phosphorylation may inhibit this interaction.

To validate MKlp2's microtubule binding via the C-terminal tail in vivo, motorless phosphoresistant mutants (mCherry-MKlp2$^{510–890/C\text{-}4A}$ and mCherry-MKlp2$^{710–890/C\text{-}3A}$) were transiently expressed in STLC-arrested HeLa cells. These phosphoresistant mutants sufficiently localized to monopolar spindles (Figure 2I, subpanels c and d). In contrast, mCherry-MKlp2^{WT} was largely restrained in the cytoplasm (subpanel a), and mCherry-MKlp2$^{510–890}$ was localized in the cytoplasm as well as weakly to chromosomes (subpanel b). Thus, the C-terminal tail of MKlp2 also mediates microtubule binding in vivo, while Cdk1/cyclin B1-dependent phosphorylation inhibits this activity. Notably, the stalk domain was required for chromosome targeting, because mCherry-MKlp2$^{510–890/C\text{-}4A}$, but not MKlp2$^{710–890/C\text{-}3A}$, also localized to chromosomes (Figure 2I, subpanels c and d). This was evident when microtubules were depolymerized by Noco treatment (Figure 2J). Taken together, we conclude that the stalk and C-terminal tail domains represent the cryptic microtubule binding, higher-order complex formation, and chromosome targeting sites in MKlp2, whereas Cdk1/cyclin B1 phosphorylation may inhibit these abilities of MKlp2.

Cdk1/Cyclin B1-Dependent Phosphorylation Inhibits MKlp2 for Proper Early Mitotic Progression

Next, we determined the effects of premature microtubule binding of MKlp2 on spindle dynamics using fluorescence recovery after photobleaching (FRAP) analysis. For this purpose, mCherry-MKlp2 was transiently expressed in STLC-arrested HeLa cells stably expressing GFP-α-tubulin. Notably, the dynamic exchange rate of the phosphoresistant MKlp2 mutants (MKlp2^{7A} and MKlp2$^{C\text{-}4A}$) between the monopolar spindles and cytoplasm was slower than MKlp2^{WT} (Figures 3A–3C), indicating a stable binding to spindles. Moreover, these mutants markedly decreased the turnover rate of monopolar spindles (Figures 3A, 3B, and 3D). Thus, these mutants alter spindle dynamics, possibly by enhancing microtubule stability.

Proper spindle dynamics are essential for bipolar spindle formation and chromosome congression (reviewed by Meunier and Vernos, 2012). When HeLa cells stably expressing GFP-histone H2B (chromosome marker) were released from STLC-induced mitotic arrest, transiently expressed mCherry-MKlp2^{WT} was largely present in the cytoplasm until the completion of chromosome congression, while it localized to chromosomes and subsequently to the midzone in anaphase (Figure 3E; Movie S1). In contrast, mCherry-MKlp2$^{C\text{-}4A}$ strongly bound to microtubules and disrupted chromosome congression (Figures 3F and 3G; Movies S2 and S3 including MKlp2^{7A}), while the phosphomimetic mutant MKlp2$^{C\text{-}4E}$ did not (Movie S4). Moreover, Dox-induced phosphoresistant mutants of Flag-MKlp2 also markedly increased the number of cells with misaligned chromosomes (Figure 3H; see also Figure 1G, subpanel b). Of note, given the essential role of the CPC in chromosome congression, it is possible that MKlp2$^{C\text{-}4A}$ may also perturb the CPC in regulating chromosome congression. Nonetheless, these results suggest that Cdk1/cyclin B1-dependent phosphorylation inhibits MKlp2 for proper early mitotic progression.

Cdk1/Cyclin B1 Inhibits MKlp2's Oligomerization/Clustering and Microtubule Bundling In Vitro

To directly investigate whether MKlp2 induces oligomerization/clustering and microtubule bundling in a Cdk1/cyclin B1-dependent manner in vitro, recombinant full-length MKlp2^{WT} and nonphosphorylatable mutant MKlp2^{7A} were purified to near homogeneity using a baculovirus expression system (Figure 4A). Inclusion of purified Cdk1/cyclin B1 efficiently phosphorylated MKlp2^{WT}, but not MKlp2^{7A}, as determined using phosphospecific antibodies (Figure 4B, lanes 5–8). Notably, MKlp2^{WT} and MKlp2^{7A} became equally insoluble only in low-ionic-strength solutions (Figure 4C, top panels, lane 2), suggesting that this insolubility was charge dependent. Importantly, Cdk1/cyclin B1 phosphorylation significantly increased solubility of MKlp2^{WT}, but not MKlp2^{7A} (Figure 4C, bottom panels, lane 2), suggesting that Cdk1/cyclin B1 phosphorylation controls solubility of MKlp2. Moreover, as determined by sucrose density gradient centrifugation, MKlp2^{WT} and MKlp2^{7A} in low-ionic-strength solutions were found in the fractions 5–7 (Figure 4D, middle panels), while both proteins migrated much slower in high-ionic-strength solutions (top panels), indicating oligomerization/clustering of MKlp2 in a charge-dependent manner. Notably, Cdk1/cyclin B1 phosphorylation also significantly slowed migration of MKlp2^{WT}, but not MKlp2^{7A}, in low-ionic-strength solutions (Figure 4D, bottom panels). Of note, sucrose might be inhibitory for oligomerization/clustering of MKlp2 as increasing sucrose concentration

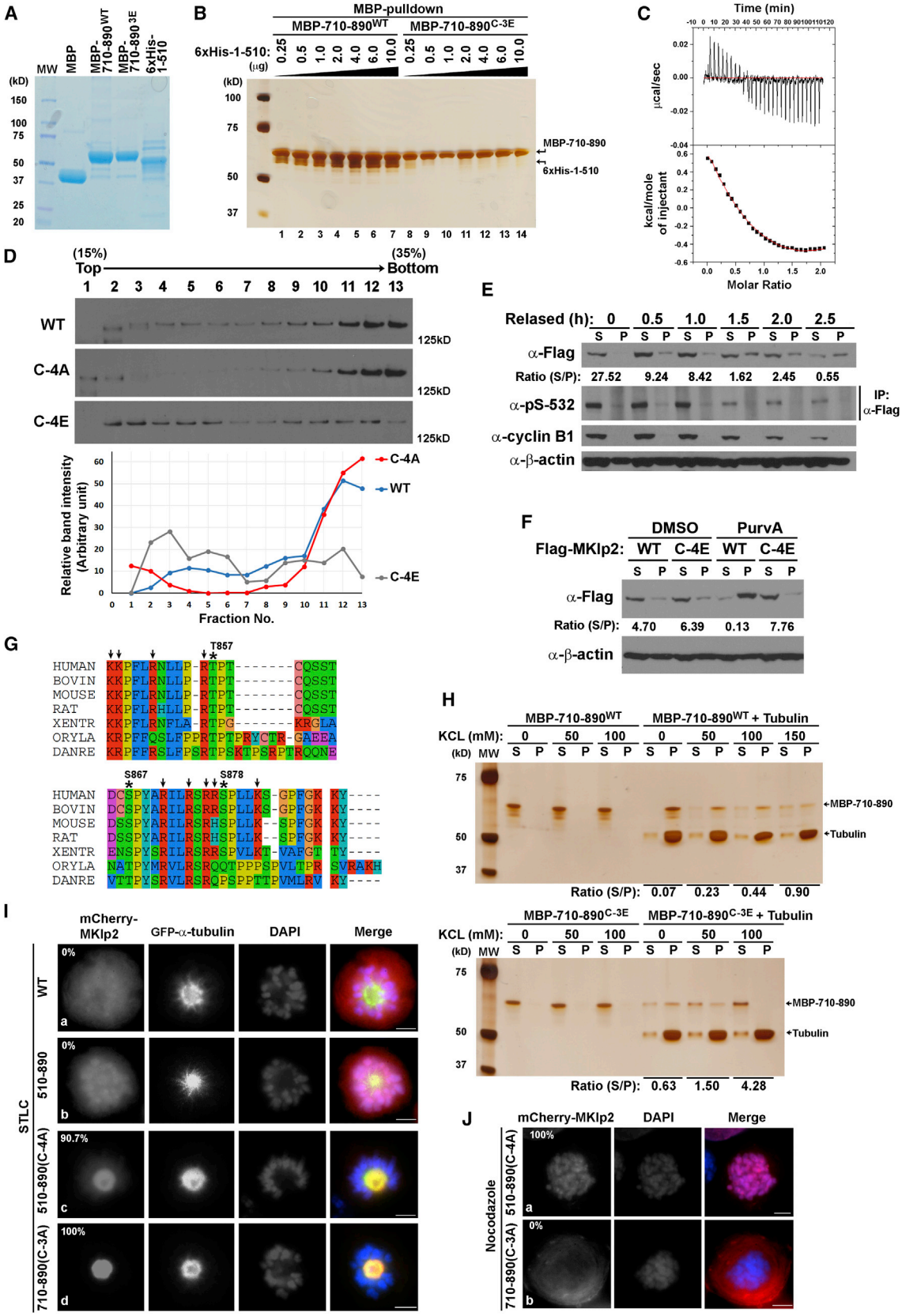

(legend on next page)

promoted solubility of MKlp2^{WT} (Figure S3), indicating that the sedimentation coefficient of MKlp2 (Figure 4D) is likely underrepresented. Nonetheless, these results suggest that Cdk1/cyclin B1 phosphorylation inhibits MKlp2's oligomerization/clustering. Moreover, Cdk1/cyclin B1 phosphorylation also suppressed the in vitro microtubule bundling activity of MKlp2^{WT}, but not MKlp2^{7A} (Figures 4E and 4F). Together with time-lapse live-cell analysis (Figure 3), these results suggest that Cdk1/cyclin B1-mediated phosphorylation may prevent MKlp2 from perturbing spindle dynamics for proper early mitotic progression.

Cdk1/Cyclin B1-Dependent Phosphorylation Controls Timely Recruitment of MKlp2 to Chromosomes

Although small interfering RNA (siRNA)-mediated knockdown of MKlp2 blocks CPC relocation from anaphase chromosomes (Gruneberg et al., 2004), how the spatial recognition between MKlp2 and the CPC occurs is unknown. Notably, although endogenous MKlp2 localized in the cytoplasm and weakly to chromosomes in Noco-arrested HeLa cells, PurvA treatment markedly recruited MKlp2 to chromosomes, whereas pretreating with calyculin A (CalA) to inhibit the major Ser/Thr phosphatases PP1/PP2A was able to exclude MKlp2 from chromosomes even after PurvA treatment (Figures 5A and 5B). Thus, Cdk1/cyclin B1 and PP1/PP2A regulate MKlp2's chromosome targeting. Similarly, mCherry-MKlp2$^{C\text{-}4A}$ constitutively localized to chromosomes (and also to the cell cortex) in Noco-arrested HeLa cells, while mCherry-MKlp2$^{C\text{-}4E}$ was excluded from chromosomes (Figure 5C). Moreover, live-cell time-lapse microscopy analysis revealed that mCherry-MKlp2^{WT} targeted to chromosomes immediately after PurvA treatment, whereas neither mCherry-MKlp2$^{C\text{-}4A}$ nor mCherry-MKlp2$^{C\text{-}4E}$ was sensitive to PurvA treatment (Figure 5D; Movie S5). Consistently, FRAP analysis revealed that the dynamic exchange rate of the phosphoresistant mutants between chromosomes and the cytoplasm in Noco-arrested HeLa cells was slower than wild-type (Figure 5E–5H). Of note, this chromosome targeting may be via the core histones, because affinity purification using the minimal chromosome binding motif of MKlp2 (Figure 6I) showed that nearly stoichiometric amounts of histone polypeptides were detected in mass spectrometry analysis after SDS-PAGE and silver staining (M.K. and S.H.L., unpublished data). Thus, we conclude that Cdk1/cyclin B1-dependent phosphorylation controls timely recruitment of MKlp2 to chromosomes where the spatial recognition between MKlp2 and the CPC may occur.

Reversing Cdk1/Cyclin B1-Dependent Phosphorylation of MKlp2 Is Necessary for Relocating the CPC from Anaphase Chromosomes to the Cell Equator for Cytokinesis

Our findings revealed that Cdk1/cyclin B1-dependent inhibitory phosphorylation of MKlp2 is essential for proper early mitotic progression. Next, we tested whether reversing this inhibitory phosphorylation is required for MKlp2's function in relocating the CPC during anaphase progression. As expected, the knockdown of endogenous MKlp2 completely blocked Aurora B relocation from anaphase chromosomes, while Dox-induced siRNA-resistant Flag-MKlp2^{WT} efficiently rescued it (Figure 6A, subpanels a and b; Figure 6B). In contrast, Dox-induced phosphomimetic mutant Flag-MKlp2$^{C\text{-}4E}$ localized to neither anaphase chromosomes nor the cell equator, and it failed to relocate Aurora B from anaphase chromosomes in MKlp2-depleted cells (Figure 6A, subpanels c and d; Figure 6B), leading to the increased number of binucleated cells from failed cytokinesis (Figure 6C). Notably, this defect was not due to a failure in reversing inhibitory phosphorylation of INCENP at the Thr-59 residue in anaphase (Figure S5A). Moreover, a directed two-hybrid assay revealed that MKlp2^{WT} and MKlp2$^{C\text{-}4A}$ efficiently interacted with INCENP, while the phosphomimetic MKlp2$^{C\text{-}4E}$ failed to do so (Figure 6D, top panel), despite comparable expression of MKlp2$^{C\text{-}4E}$ to MKlp2^{WT} in cell lysates from yeast (bottom panel). Similarly, as determined by immunoprecipitation analysis using Noco-arrested HeLa cells, Dox-induced Flag-MKlp2^{WT} efficiently bound to INCENP and Aurora B upon inactivation of Cdk1 (Figure 6E, lanes 5 and 6), whereas Flag-MKlp2$^{C\text{-}4E}$ did not (lanes 7 and 8). Notably, a directed two-hybrid assay revealed that the N-terminal domain of INCENP encompassing aa 1–58 (INCENP$^{1\text{-}58}$) was responsible for binding

Figure 2. Phosphoregulation of MKlp2's Higher-Order Complex Formation, Direct Microtubule Binding, and Chromosome Targeting

(A) Coomassie blue staining of purified recombinant proteins from *E. coli*.

(B) Silver staining of 6xHis-MKlp2 motor domain precipitates with the indicated MBP-MKlp2 tail domains.

(C) Isothermal titration calorimetry (ITC) assay. The record of heat exchange (top) and the fitted binding isotherm assuming a sequential binding model (bottom) are shown.

(D) Lysates of asynchronously growing HeLa cells expressing the indicated mCherry-MKlp2 were subjected to sucrose gradient sedimentation. Fractions were removed from the top (lane 1), separated by SDS-PAGE, and immunoblotted with α-mCherry antibodies (top panels). The quantification results of band intensities in each fraction are plotted (bottom graph).

(E and F) Noco-arrested HeLa cells with Dox-induced Flag-MKlp2 were harvested at indicated times after synchronously released (E) or treated with PurvA (F). Flag-MKlp2 in supernatant (S) and pellet (P) fractions was analyzed by immunoblot. For α-pS532, total cell lysates were subjected to immunoprecipitation using α-Flag antibodies (E).

(G) Sequence alignment (Clustal Omega) of the C-terminal tail of MKlp2 with homologs from different species. Asterisks indicate Cdk1/cyclin B1 phosphosites with amino acid numbers. Arrows indicate conserved basic Arg/Lys/His residues.

(H) Purified recombinant MBP-MKlp2 tail domains in increasing concentrations of KCl were incubated with or without taxol-stabilized microtubules and ultracentrifuged. The equal percentages of resulting supernatant (S) and pellet (P) fractions (10% of total) were analyzed by silver staining. The band intensity ratios (S/P) between the supernatant and pellet fractions are indicated (E), (H).

(I and J) HeLa cells stably expressing GFP-α-tubulin were transfected with expression vectors encoding the indicated mCherry-MKlp2 for 6 hr. The cells were subsequently treated with STLC (I) or Noco (J) for 16 hr. The percentages of cells with mCherry-MKlp2 strongly localized to monopolar spindles (I) or chromosomes (J) are indicated (n > 100 cells per condition).

White bars in (I) and (J) represent 5 μm.

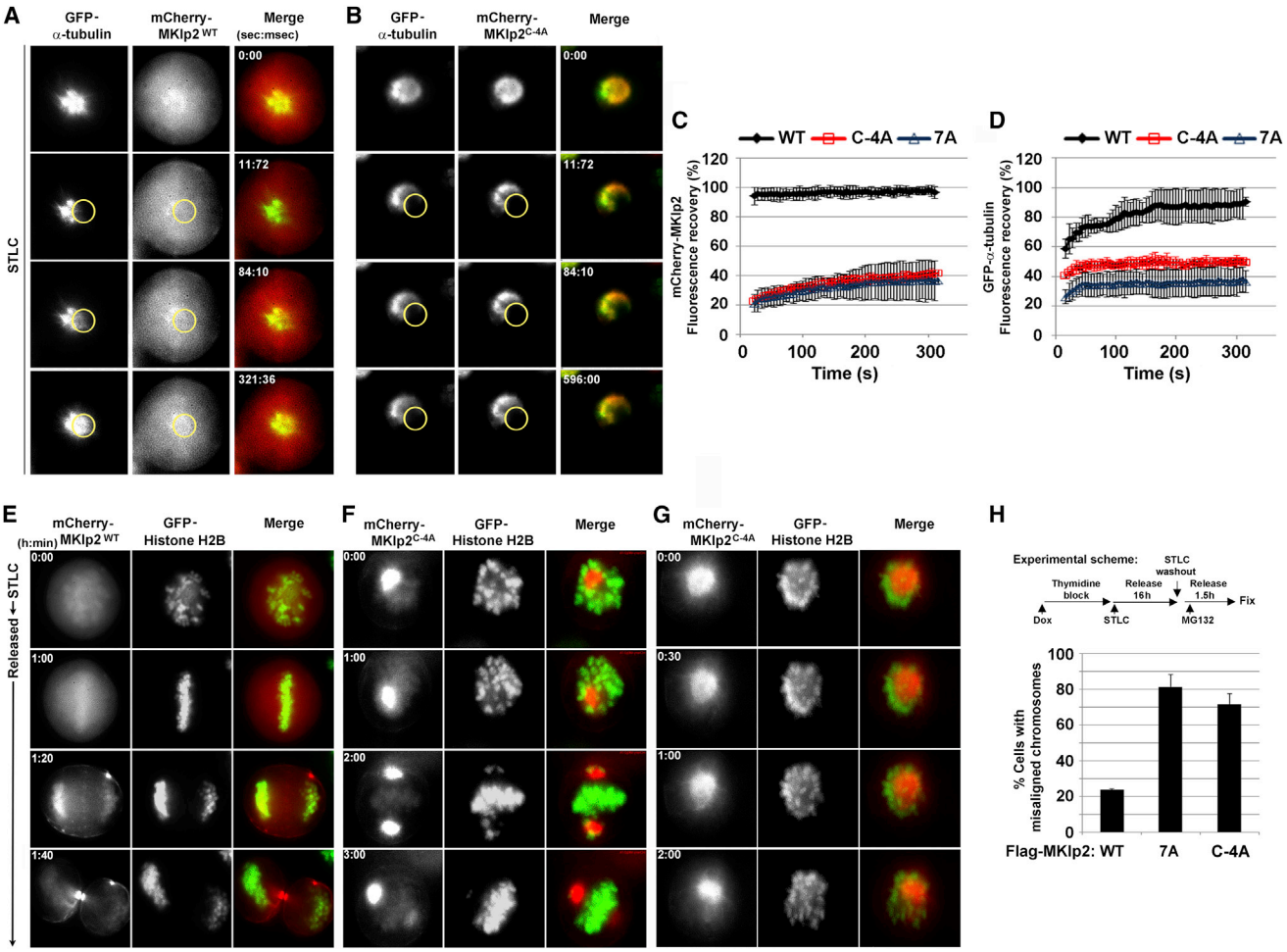

Figure 3. Cdk1/Cyclin B1-Dependent Phosphorylation Inhibits MKlp2's Microtubule Binding for Proper Spindle Dynamics and Chromosome Congression

(A–D) FRAP analysis. HeLa cells stably expressing GFP-α-tubulin were transfected with expression vectors encoding the indicated siRNA-resistant mCherry-MKlp2 together with MKlp2 siRNA for 6 hr and subsequently treated with STLC for 16 hr. A selected area of the cell (yellow circle) was photobleached with the λ = 543 and λ = 488 laser lines (A and B), and FRAP was measured as the increase of mCherry-MKlp2 and GFP-α-tubulin fluorescence after photobleaching in the selected area. (C and D) The average percentages of fluorescence recovery (n = 5 cells per condition, ±SD) are shown.

(E–G) Time-lapse live-cell images. HeLa cells stably expressing GFP-histone H2B were transfected as described above (A–D). The cells were subsequently treated with STLC for 16 hr and released.

(H) Dox-inducible HeLa cells treated with Dox during the thymidine block were released from the G_1/S boundary and subsequently arrested using STLC treatment. Then, the cells were released in fresh medium containing MG132 for 1.5 hr to induce chromosome congression and fixed for immunofluorescence analysis. The average percentages based on three independent experiments of cells expressing Flag-MKlp2 with misaligned chromosomes (n > 100 per condition, ±SD) are shown.

MKlp2^{WT}, while it failed to bind MKlp2^{C-4E} (Figure 6F). Furthermore, recombinant glutathione S-transferase (GST)-tagged INCENP$^{1–58}$ purified from *E. coli* (Figure 6G, lane 2) was able to bind recombinant MKlp2^{WT} and MKlp2^{7A} (lanes 3 and 4), while Cdk1/cyclin B1 phosphorylation of MKlp2^{WT}, but not MKlp2^{7A}, inhibited this interaction in vitro (lanes 7 and 8). Of note, both INCENP^{WT} and INCENP^{T59E} comparably interacted with MKlp2^{WT} in a directed two-hybrid, quantitative β-galactosidase and GST pull-down assay, while MKlp2^{C-4E} failed to bind INCENP^{WT} and INCENP^{T59E} in immunoprecipitation assay (Figures S5B–S5D). Thus, these results indicate that reversing Cdk1/cyclin B1-dependent phosphorylation of MKlp2 may promote the formation of a CPC:MKlp2 complex (possibly via INCENP) to mediate CPC relocation for cytokinesis.

To further test the importance of reversing the phosphoinhibition of MKlp2 in CPC relocation, hemagglutinin (HA)-tagged phosphoresistant INCENP (HA-INCENP^{T59A}) was transiently expressed in Dox-induced HeLa cells expressing Flag-MKlp2. Although Dox-induced Flag-MKlp2^{WT} efficiently relocated to the cell equator together with HA-INCENP^{T59A}, Flag-MKlp2^{C-4E} was unable to remove HA-INCENP^{T59A} from anaphase chromosomes (Figure 6A, subpanels e and f), indicating that reversing the inhibitory phosphorylation of MKlp2 is required for relocating INCENP independent of dephosphorylation at the Thr-59

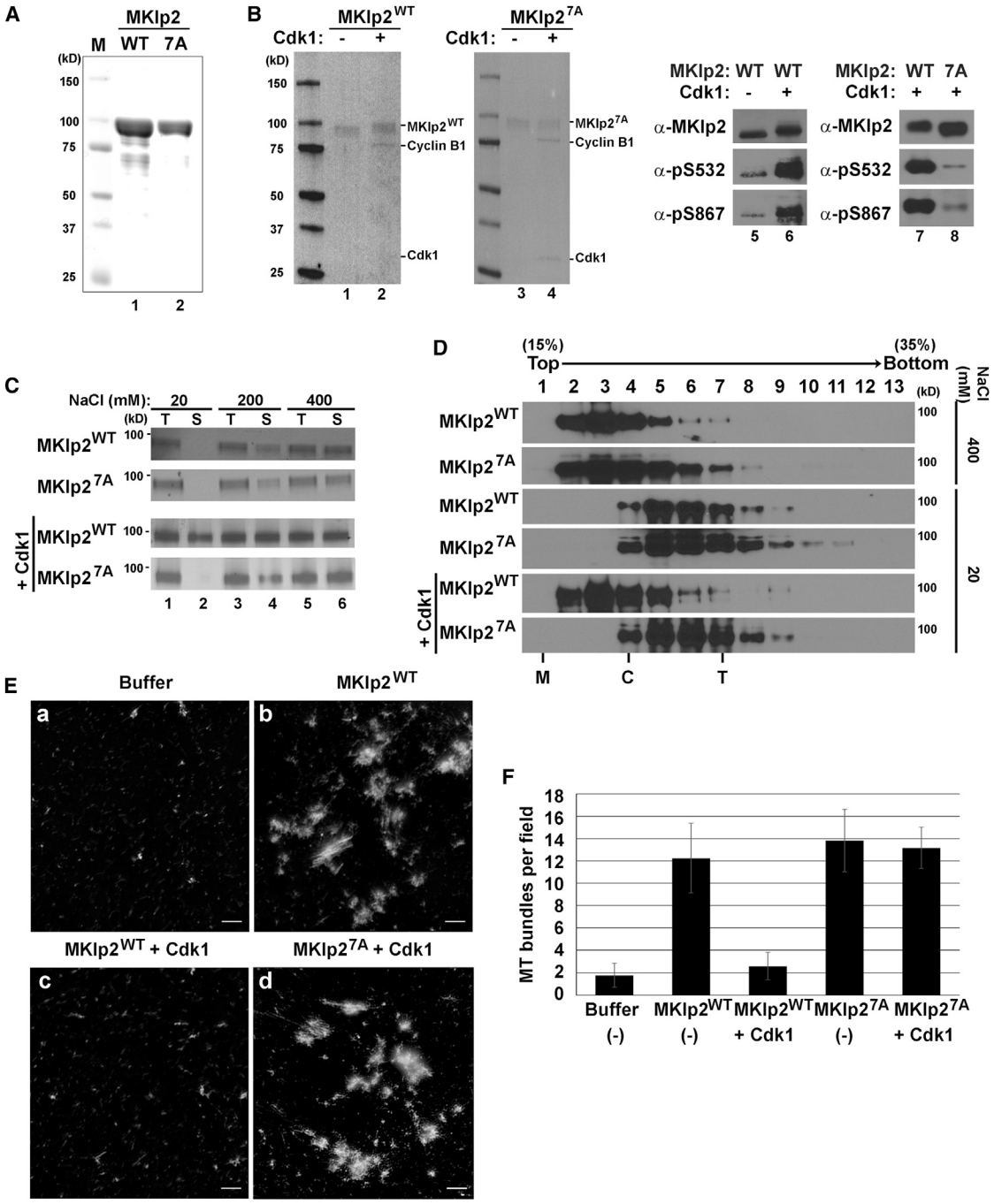

Figure 4. Cdk1/Cyclin B1 Inhibits MKlp2's Oligomerization/Clustering and Microtubule Bundling In Vitro

(A) Coomassie blue staining of purified recombinant full-length MKlp2^{WT} and MKlp2^{7A} from Sf9 cells.

(B) Purified MKlp2 proteins (0.25 μg) were subjected to in vitro kinase assay with or without active Cdk1/cyclin B1 (0.1 μg). Phosphorylated MKlp2 was evaluated by Coomassie blue staining (lanes 1–4) and immunoblot analysis (lanes 5–8) using indicated phosphospecific antibodies.

(C) Solubility of phosphorylated or nonphosphorylated MKlp2 was assayed after dilution into buffers with increasing concentrations of NaCl and analyzed by silver staining. T, total; S, supernatant.

(D) Sucrose gradient sedimentation of phosphorylated or nonphosphorylated MKlp2. Fractions were removed from the top (lane 1) and analyzed with immunoblot using α-MKlp2 antibodies. The sedimentation of the size standards malate (M; 4.3 S), catalase (C; 11.3 S), and thyroglobulin (T; 19.3 S) is indicated (bottom).

(E) Microtubule bundling assay. The panels show the distribution of microtubules. White bars represent 5 μm.

(F) The extent of microtubule bundling was quantified from ten random fields of samples (E) and the number of microtubules bundled per field were counted. The average numbers of microtubules bundled per conditions (±SD) are shown.

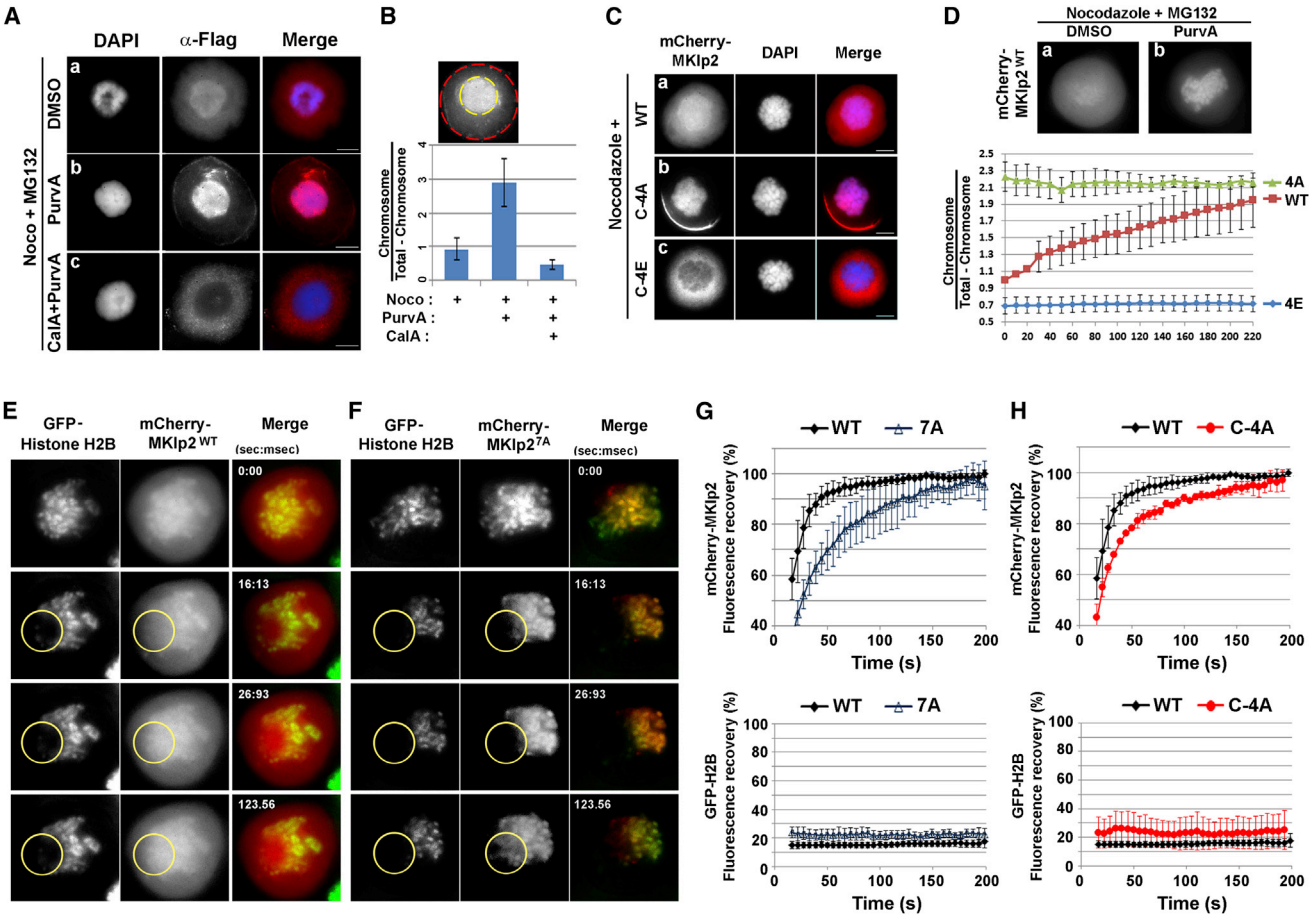

Figure 5. Cdk1/Cyclin B1 Inhibits MKlp2 Targeting to Chromosomes

(A) Noco-arrested HeLa cells were treated with MG132 for 1 hr (a–c) and then with DMSO (subpanel a) or PurvA (subpanel b) before fixing in ice-cold methanol. For subpanel c, the cells were treated with CalA before the addition of PurvA.

(B) Quantification of the chromosome localization of endogenous MKlp2. The ratio (n = 10 per condition, ±SD) of the chromosome fluorescence to non-chromosome fluorescence was calculated as described in the y axis legend. The inset shows MKlp2 concentrates on chromosomes in Noco-arrested HeLa cells after PurvA treatment. Circles indicate regions used for the quantification of the extent of chromosome localization (yellow) and total localization (red).

(C and D) HeLa cells were transfected with expression vectors encoding the indicated mCherry-MKlp2 for 6 hr and subsequently treated with Noco for 16 hr. (C) The cells were fixed in ice-cold methanol. (D) The cells were treated with MG132 for 1 hr. Upon DMSO (subpanel a) or PurvA (subpanel b) treatment, the accumulation of mCherry-MKlp2 on chromosomes was monitored with time-lapse live-cell microscopy analysis (top) and quantified (bottom, n = 10 cells per condition, ±SD).

(E–H) FRAP analysis. HeLa cells stably expressing GFP-histone H2B were transfected with expression vectors encoding the indicated siRNA-resistant mCherry-MKlp2 together with MKlp2 siRNA for 6 hr. The cells were subsequently treated with Noco for 16 hr. A selected area of the cell (yellow circle) was photobleached with the λ = 543 and λ = 488 laser lines (E and F), and FRAP was measured as the increase of mCherry-MKlp2 and GFP-histone H2B fluorescence after photobleaching in the selected area. (G and H) The average percentages of fluorescence recovery (n = 5 cells per condition, ±SD) are shown.

residue. Furthermore, when these cells were subsequently arrested in the monopolar state by STLC and briefly treated with PurvA (Canman et al., 2003), Flag-MKlp2^{WT} relocated together with HA-INCENP^{T59A} to the monopolar spindles (Figure 6H, subpanel b). In contrast, CalA treatment prevented Flag-MKlp2^{WT} from relocating HA-INCENP^{T59A} from chromosomes (Figure 6H, subpanel c). Under this condition, Flag-MKlp2^{WT} was restrained in the cytoplasm (Figure 6H, subpanel c), similar to Flag-MKlp2^{C-4E} in anaphase (Figure 6A, subpanels d and f). Together, these results suggest that reversing Cdk1/cyclin B1-dependent phosphorylation allows MKlp2 to relocate the CPC.

Finally, to test whether MKlp2's chromosome targeting indeed contributes to CPC relocation from anaphase chromosomes, we identified that amino acid residues encompassing 510–840 (MKlp2$^{510–840}$) were sufficient for MKlp2's chromosome targeting, but not microtubule binding (Figure 6I; Figure S4). Notably, using HeLa cells stably expressing mCherry-tagged Aurora B, transiently targeting GFP-MKlp2$^{510–840}$ to chromosomes markedly suppressed mCherry-Aurora B relocation from anaphase chromosomes, while GFP-histone H2B (as chromosome targeting control) did not (Figure 6J). This indicates that MKlp2$^{510–840}$ may outcompete endogenous MKlp2 for recognition of the CPC at anaphase chromosomes. Taken together, we conclude

that reversing Cdk1/cyclin B1-mediated inhibitory phosphorylation contributes to timely activation of MKlp2 and relocation of the CPC (possibly via INCENP) from anaphase chromosomes. Furthermore, this event promotes MKlp2's abilities for microtubule binding and bundling as well as oligomerization/clustering, which may contribute to central spindle assembly/stabilization and clustering/activation of the CPC at the cell equator for robust furrow ingression (Figure 7). Thus, this key phosphoregulatory step connects early and late mitotic events for proper mitotic progression.

DISCUSSION

Here, we show that several aspects of MKlp2 kinesin function are negatively regulated by Cdk1/cyclin B1-dependent phosphorylation. Notably, the C-terminal basic stretches of MKlp2 directly interact with tubulin (possibly via C-terminal "E-hook" acidic tail), while Cdk1/cyclin B1 phosphosites embedded in these basic stretches would inhibit MKlp2's microtubule binding during early mitosis, similar to MKlp1/ZEN-4 (Mishima et al., 2004). Likewise, the N-terminal unstructured basic tail of Ndc80, the microtubule binding element of kinetochore, mediates high-affinity microtubule binding (Ciferri et al., 2008; DeLuca et al., 2006; Guimaraes et al., 2008; Miller et al., 2008; Wei et al., 2007), which is inhibited by Aurora B phosphorylation (Alushin et al., 2012). Similarly, the C-terminal Lys/Arg-rich domain of PRC1 enhances microtubule binding and crosslinking antiparallel microtubules for central spindle formation (Subramanian et al., 2010), while this unstructured domain is subjected to Cdk1/cyclin B1 phosphoregulation (Zhu et al., 2006). Based on protein secondary structure prediction, the C-terminal tail of MKlp2 is unstructured. Thus, it is conceivable that this unstructured tail could provide a wide range of orientations and functions. Indeed, we show that this C-terminal tail also forms a complex with its motor domain in patterns of sequential interaction. Thus, upon initial contact with the motor domain, the unstructured C-terminal tail of MKlp2 may induce conformation adaptation to promote intimate complex formation in a head-to-tail geometry, thus clustering. Similarly, the disordered N-terminal tail of Ndc80 interacts with the E-hook of tubulin and induces Ndc80 clustering (Alushin et al., 2010, 2012), suggesting that microtubule binding and cluster formation are intimately connected.

We also show that Cdk1/cyclin B1 phosphorylation inhibits oligomerization/clustering and microtubule bundling of MKlp2 in order to avoid premature stabilization and bundling of microtubules that causes defects in chromosome congression in early mitosis. In anaphase, however, Cdk1/cyclin B1-dependent inhibitory phosphorylation must be reversed by PP1/PP2A for timely activation of MKlp2. This mechanism may be a way for clustered MKlp2 at microtubule plus ends to capture and bundle antiparallel microtubules near the cortical equator. Furthermore, multimerized MKlp2 may also stably cluster and activate the CPC at the cell cortex and subsequently at the actomyosin filaments for robust furrow ingression (Kitagawa et al., 2013). Evidently, the mechanism by which the CPC and clustered MKlp2 complex engage microtubule plus ends and ingressing furrow is an important area for future research.

Our findings also suggest that the spatiotemporal recognition between MKlp2 and the CPC may occur at anaphase chromosomes. Notably, we show that MKlp2 dynamically localizes to chromosomes. This event is also inhibited by Cdk1/cyclin B1 that is opposed by PP1/PP2A. Moreover, when the motif responsible for MKlp2's chromosome targeting is ectopically expressed, it blocks Aurora B relocation from anaphase chromosomes, suggesting that MKlp2 may remove the CPC from anaphase chromosomes. However, this preferential chromosome targeting of MKlp2 upon inhibition of Cdk1 is unexpected, because the phosphoresistant mutant binds microtubules much stronger than chromosomes based on our FRAP analysis. This difference may be explainable if the phosphatase activity relevant to MKlp2 is highly present at chromosomes. Alternatively, the phosphoresidues in the stalk and C-terminal tail domains may be dephosphorylated sequentially so that chromosome targeting would occur prior to microtubule binding. It is also possible that Plk1 phosphorylation (Neef et al., 2003) may also affect MKlp2 localization in mitotic progression. Nonetheless, the preferential recruitment of MKlp2 to anaphase chromosomes may be a regulatory means to achieve a spatial recognition between MKlp2 and the CPC without perturbing microtubule dynamics (or bundling mitotic spindles and/or kinetochore fibers to metaphase spindles). Subsequently, this spatial regulatory event may assist MKlp2 to transport the CPC from anaphase chromosomes to microtubules in a temporal manner. This idea is consistent with a notion that a subpopulation of stable microtubules extends past chromosomes, which may supply microtubule stability and furrowing factors from chromosomes to the cortex (Canman et al., 2003).

We also propose that reversing Cdk1/cyclin B1-mediated phosphorylation of MKlp2 is an essential regulatory step to recognize the CPC possibly via INCENP. This conclusion is supported by the following results: (1) the inhibitory phosphorylation of MKlp2 is rapidly reversed upon anaphase onset, (2) the phosphomimetic mutant neither binds INCENP nor relocates the CPC regardless INCENP phosphorylation at the Thr-59 residue, and (3) blocking MKlp2 dephosphorylation by inhibiting PP1/PP2A also inhibits relocating INCENP^{T59A} from chromosomes. Although the reason why Cdk1/cyclin B1 phosphoregulates both MKlp2 (in this study) and INCENP (Goto et al., 2006; Hümmer and Mayer, 2009) is unclear, our results suggest that reversing the inhibitory phosphorylation of MKlp2 may be required for the interaction between MKlp2 and the CPC (possibly via INCENP). Alternatively, INCENP dephosphorylation at the Thr-59 may be required for MKlp2 to recognize the CPC as a complex or for the relocation step from anaphase chromosomes independent of forming the CPC:MKlp2 complex.

In summary, timely activation of MKlp2 by Cdk1/cyclin B1-mediated phosphoregulation is an essential mechanism to coordinate the events required for proper mitotic progression and relocating the CPC for cytokinesis. Furthermore, our findings suggest that Cdk1/cyclin B1 regulates functions of MKlp2 for proper mitotic progression, raising a possibility that misregulated or overexpressed MKlp2 in many human cancers may contribute to chromosome instability and tumorigenesis. Future research efforts will be required for a more detailed elucidation of the exact underlying mechanisms.

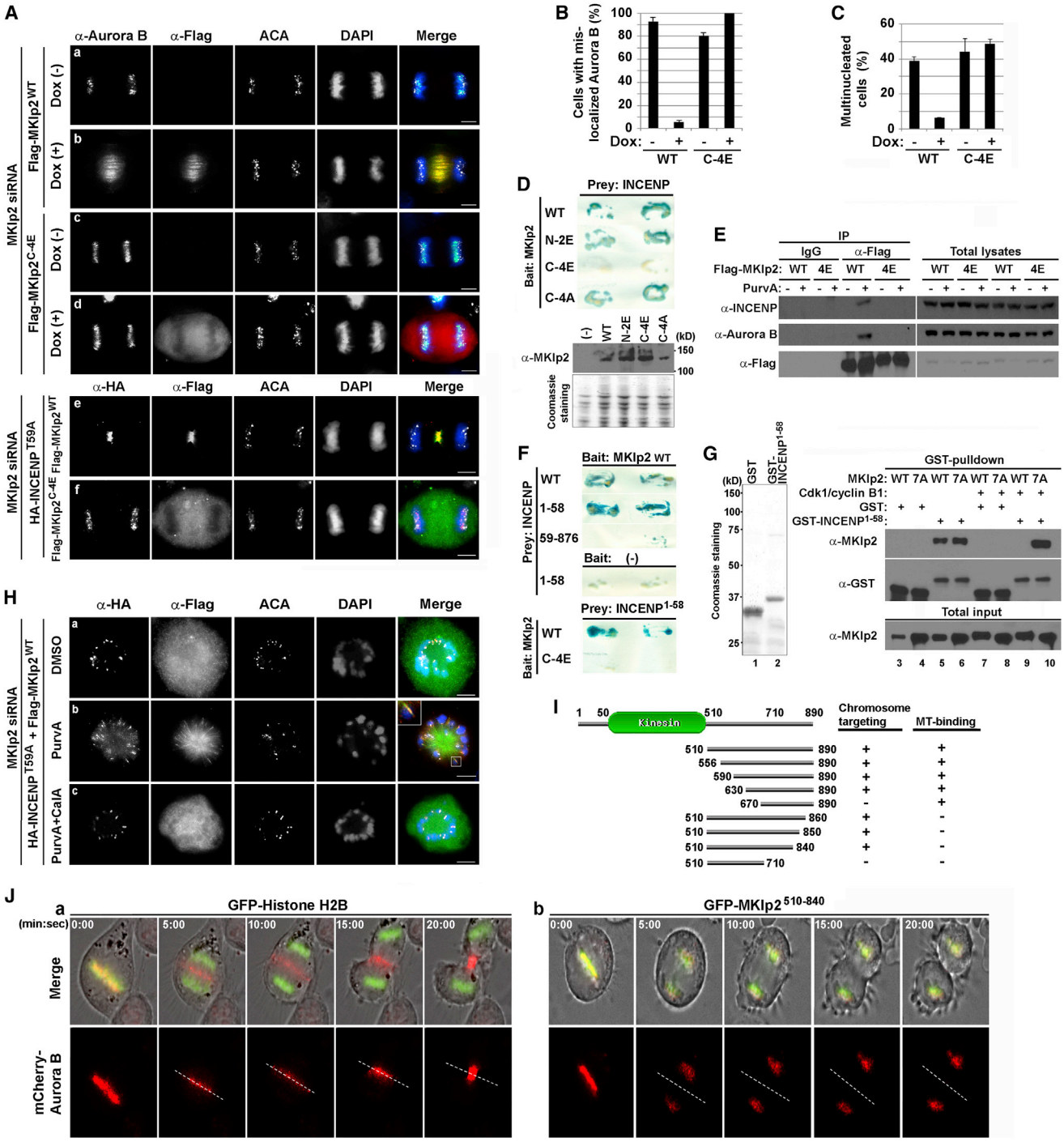

Figure 6. Reversing Cdk1/Cyclin B1-Dependent Phosphorylation of MKlp2 Is Necessary for Relocating the CPC from Anaphase Chromosomes to the Cell Equator for Cytokinesis

(A and H) Immunofluorescence analysis. Dox-inducible HeLa cells were transfected for 4 hr with siRNA against MKlp2. Subsequently, the cells were treated with Dox for 26 hr before fixing in ice-cold methanol. For (A) (subpanels e and f) and (E), expression vectors encoding HA-INCENP^{T59A} were transfected together with siRNA against MKlp2.

(B and C) Quantification of the average percentages of cells with Aurora B that failed to relocate to the cell equator (B) and became multinucleated due to cytokinesis failure (C) (n > 100 cells per condition, ±SD).

(D and F) Yeast two-hybrid assay. The interaction between MKlp2 and INCENP was evaluated by colony growth as well as β-galactosidase staining assay. (D, bottom panels) The expression levels of MKlp2 were determined by immunoblot analysis using α-MKlp2 antibodies and Coomassie blue staining (loading control).

(legend continued on next page)

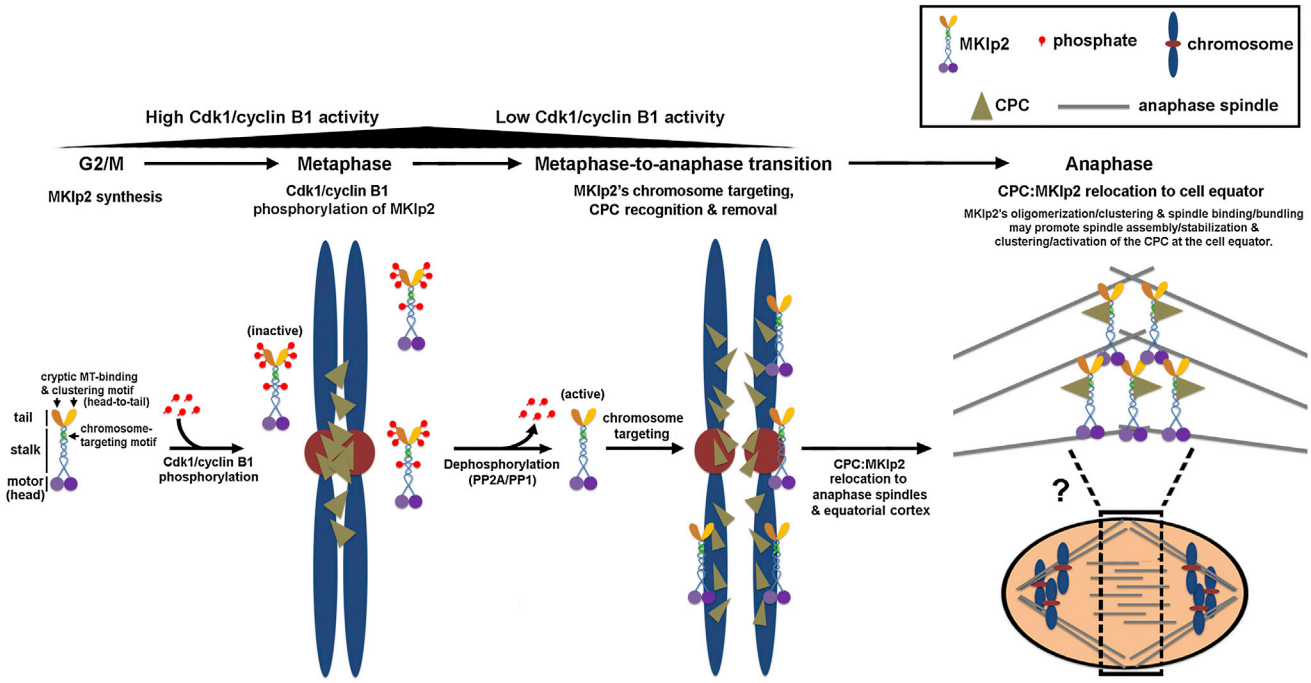

Figure 7. Proposed Model

Cdk1/cyclin B phosphorylates multiple sites in the stalk and C-terminal tail domains of MKlp2 in early mitosis. This phosphorylation inhibits MKlp2's microtubule binding, oligomerization/clustering, and recruitment to chromosomes. Upon anaphase onset, however, reversing Cdk1/cyclin B1-mediated inhibitory phosphorylation is necessary for the timely promotion of MKlp2's kinesin function and relocation of the CPC from anaphase chromosomes to the cell equator, possibly via INCENP binding. Subsequently, it promotes MKlp2's abilities for microtubule binding and bundling as well as oligomerization/clustering that may contribute to central spindle assembly/stabilization and clustering/activation of the CPC at the cell equator. This clustering event may also stably deliver the CPC near to the cell cortex for robust furrow ingression.

EXPERIMENTAL PROCEDURES

Cell Lines, Culture, and Reagents

HeLa cells including stably expressing GFP-α-tubulin, GFP-histone H2B, or mCherry-Aurora B were maintained in Dulbecco's modified Eagle's medium with 10% fetal bovine serum (Invitrogen). Vectors encoding HA-, Flag-, and mCherry-tagged MKlp2 were previously described (Lee et al., 2010; Kitagawa et al., 2013). For Figure 6I, indicated MKlp2 cDNAs were amplified and cloned into the pEGFP-C1 vector. Site-directed mutagenesis was performed with the use of a site-directed mutagenesis system (Gene Tailor; Invitrogen) and verified by sequencing. The Dox-inducible system and siRNAs were previously described (Kitagawa et al., 2013). Antibodies used for immunoblot and immunofluorescence analysis are described in Supplemental Experimental Procedures.

Cell Synchronization, Immunoprecipitation, and Immunoblot Analysis

For Figures 1A–1C, 1E, and 1J, HeLa cells were synchronized at the G_1/S boundary by exposure to 2 mM thymidine for 16 hr and incubated in fresh medium for 10 hr. After the second thymidine block for 14 hr, cells were released in fresh medium containing Noco (200 ng/ml) for 12 hr. From the second thymidine block, Dox (5 μg/ml) was added. For Figures 1B and 1J, the cells were collected by mitotic shake-off, washed in PBS, released in fresh medium, and collected at the indicated time points. For Figures 1A, 1J, 2F, and 6E, Noco-arrested cells were briefly treated with either DMSO or PurvA (30 μM; Sigma) for 5 min before harvesting. Proteins were isolated with 1% NP-40 lysis buffer (50 mM Tris HCl [pH 8.0], 150 mM NaCl, and 1% NP-40) containing 1 mM dithiothreitol (DTT), protease inhibitor mix (Complete Mini, Roche), and PhosphoStop (Roche) and immunoprecipitated with 1 μg of antibodies

(E) Noco-arrested HeLa cells with indicated Dox-induced Flag-MKlp2 were harvested after treatment with DMSO or PurvA. Total cell lysates were subjected to immunoprecipitation using α-Flag antibodies followed by immunoblot analysis.

(G) Coomassie blue staining of purified recombinant proteins from *E. coli* (lanes 1 and 2). Purified MKlp2 proteins (0.1 μg) were subjected to in vitro kinase assay with or without active Cdk1/cyclin B1 (0.05 μg) and used for GST pull-down analysis with the indicated GST-tagged proteins (0.5 μg). The bound proteins were analyzed by immunoblot assay.

(H) After transfection and Dox treatment for 26 hr, the cells were treated with STLC, MG132, and paclitaxel to form monoasters. Where indicated, the cells were treated with CalA, PurvA, or DMSO before fixation and then subjected to immunofluorescence analysis with the indicated antibodies. Inset represents the boxed area where HA-INCENP^{T59A} relocated together with Flag-MKlp2^{WT} to the tips of monopolar spindles.

(I) Summary of the minimal motif of MKlp2 for chromosome targeting independent of microtubule binding identified in this study. HeLa cells were transfected with expression vectors encoding the indicated mCherry-MKlp2 for 6 hr. The cells were subsequently treated with STLC or Noco for 16 hr to arrest cells with monopolar spindles or depolymerized microtubules, respectively, before they were fixed with ice-cold methanol.

(J) Time-lapse live-cell images. HeLa cells stably expressing mCherry-Aurora B were transiently transfected with GFP-histone H2B or GFP-MKlp2$^{510–840}$ for 24 hr and subjected to time-lapse live-cell analysis. The images at 0:00 (min:s) were the cells at metaphase. The images from the same cells were continuously captured every 5 min as the cells progressed to anaphase.

against MKlp2 (A300-879A, Bethyl) or Flag (Wako) with Protein A/G-agarose beads (Santa Cruz) for 3 hr at 4°C. The beads were washed with 1% NP-40 lysis buffer and subjected to immunoblot analysis. For Figure 1C, Flag-MKlp2 proteins were immunopurified using FLAG M purification kit (Sigma) and treated with ALP (FastAP, Thermo Scientific) for 1 hr at 37°C. For Figures 1A–1C and 1E, Phos-tag SDS-PAGE analysis (AAL-107, Wako) was performed according to the manufacturer's instructions.

Immunofluorescence, FRAP, and Time-Lapse Live-Cell Imaging

HeLa cells grown on coverglass-bottom chamber slides (Lab Tek) were fixed with ice-cold methanol for 3 min on ice. For Figures 5A and 6H, CalA (50 nM; Sigma) was added for 15 min and PurvA (30 μM) for 2 min. The fixed cells were permeabilized with 0.5% Triton X-100 and exposed to Tris-buffered saline containing 0.1% Triton X-100 and 2% BSA (AbDil). Images including time-lapse live-cell analysis (Figures 3A–3G, 5D–5H, and 6J) were acquired with the 3D-SIM mode using a Super Resolution Microscope (Nikon) (Kitagawa et al., 2013). For FRAP analysis (Figures 3A–3D and 5E–5H), HeLa cells stably expressing either GFP-α-tubulin or GFP-histone H2B were transfected with expression vectors encoding indicated siRNA-resistant mCherry-MKlp2 together with MKlp2 siRNA for 6 hr using Turbofect transfection reagent. The cells were subsequently treated with either STLC (2.5 μM) or Noco for 16 hr before imaging. The cells were first imaged at λ = 543 to visualize mCherry-MKlp2 fluorescence and λ = 488 nm to visualize GFP-α-tubulin or GFP-histone H2B. A selected area of the cell was photobleached with the λ = 543 and λ = 488 laser lines, and FRAP was measured as the increase in mCherry-MKlp2 and GFP-α-tubulin fluorescence after photobleaching in the selected area. The data were normalized to the first prebleached image and corrected for fluorescence loss during recovery by adding back the normalized fluorescence lost from an unbleached region.

Protein Purification, MBP Pull-Down, ITC, Microtubule Binding, and Bundling Assays In Vitro

Expression and purification steps for recombinant proteins are described in Supplemental Experimental Procedures. For the MBP pull-down assay (Figure 2B), MBP-MKlp2 was loaded onto Amylose beads for 30 min at 4°C in the presence of Buffer B (80 mM PIPES [pH 7.0], 2 mM $MgCl_2$, and 0.5 mM EGTA) containing 1 mM DTT. The beads were washed with Buffer B and then incubated overnight at 4°C with 6xHis-MKlp2$^{1–510}$. The beads were washed with Buffer B and analyzed by SDS-PAGE and silver staining (Pierce). For ITC assay, the N-terminal motor domain (20 μM) was kept in the cell and the C-terminal tail (300 μM) was kept in the syringe and in a VP-ITC microcalorimeter (Microcal). For each injection, 10 μl of the C-terminal tail was injected into the cell, and the heat exchange was recorded accordingly. The dissociation constants of the N-terminal motor domain to the C-terminal tail were determined using the least-squares method, and the binding isotherm was fitted using Origin v7.0 (Microcal) assuming a sequential binding model. For the microtubule binding and sedimentation assays, 1 μg of MBP-MKlp2$^{710–890}$ proteins was supplemented with the indicated amount of KCl and taxol-stabilized microtubules (BK029; Cytoskeleton) and ultracentrifuged at 100,000 × *g* for 30 min at 25°C. The resulting supernatant (S) and pellet (P) fractions were then analyzed by silver staining. For the microtubule bundling assay, rhodamine-labeled tubulin proteins (TL590M; Cytoskeleton) were reconstituted to 4 mg/ml with Buffer B containing 1 mM guanosine triphosphate and 10 μM paclitaxel. 0.25 μg of full-length MKlp2 diluted in Buffer B was included with 4 μg of rhodamine labeled tubulin for 30 min at 25°C in a total volume of 20 μl Buffer B containing 10 μM paclitaxel and analyzed after incubation under a microscope (Nikon Eclipse Ti-E) using a 63× oil-immersion lens. Where indicated, in vitro kinase assay was performed using 0.1 μg of purified active Cdk1/cyclin B1 (Millipore) according to the manufacturer's instructions.

Sucrose Gradient Sedimentation and Fractionation

For Figure 2D, 2 μg of expression vectors encoding the indicated mCherry-MKlp2 construct was transfected into HeLa cells. At 24 hr after transfection, the cells were lysed in 200 μl buffer (80 mM PIPES [pH 7.0], 2 mM $MgCl_2$, 0.5 mM EGTA, and 0.1% Triton X-100) containing 1 mM DTT and Complete Mini and sonicated. The lysates were loaded on top of 11 ml of linear 15%–35% sucrose density gradient in PE buffer (10 mM PIPES [pH 7.2] and 1 mM EDTA) containing 0.1% Triton X-100 and ultracentrifuged in a swinging bucket SW 41 rotor (Beckman) at 37,500 rpm for 16 hr at 4°C with an acceleration and deceleration profile of 7. Fractions were removed from the top. For Figures 2E and 2F, either Noco-arrested or subsequently released HeLa cells were lysed in a low salt buffer (80 mM PIPES [pH 7.0], 50 mM NaCl, 2 mM $MgCl_2$, 0.5 mM EGTA and 0.1% Triton X-100) for 5 min and centrifuged at 13,000 rpm for 15 min. Pellets were resuspended in a high salt buffer containing NaCl (250 mM) for 5 min and centrifuged at 13,000 rpm for 15 min at 4°C. For Figures 4C and 4D, purified MKlp2 from Sf9 insect cells were diluted (final 50 μg/ml) in 80 mM PIPES (pH 7.0), 2 mM $MgCl_2$, 0.5 mM EGTA, 0.1 mM ATP, 1 mM DTT, and the indicated final concentration of NaCl and incubated for 30 min at 25°C. For Figure 4C, samples were centrifuged at 10,000 × *g* for 30 min at 25°C and the total and supernatant fractions were analyzed. For Figure 4D, samples were subjected to linear 15%–35% sucrose density gradient sedimentation at 37,500 rpm for 16 hr at 25°C. Malate dehydrogenase (4.3 S), catalase (11.3 S), and thyroglobulin (19.3 S) (Sigma) were used as standards.

Yeast Two-Hybrid Analysis

For Figures 6D and 6F, MKlp2 cDNA was cloned into the pBTM116 vector as the bait and the cDNA of INCENP were cloned into the pGAD vector as prey. Interactions were evaluated by colony growth on Trp, Leu, and His dropout plates, and a β-galactosidase assay was used for validation.

SUPPLEMENTAL INFORMATION

Supplemental Information includes Supplemental Experimental Procedures, five figures, and five movies and can be found with this article online at http://dx.doi.org/10.1016/j.celrep.2014.02.034.

ACKNOWLEDGMENTS

We thank D.M. Virshup (Duke-NUS) for critical suggestions and T. Kiyono (NCC, Japan) for the INCENP plasmid. This research is supported by the National Research Fellow programs and the Duke-NUS Graduate Medical School.

Received: August 12, 2013
Revised: November 22, 2013
Accepted: February 23, 2014
Published: March 20, 2014

REFERENCES

Alushin, G.M., Ramey, V.H., Pasqualato, S., Ball, D.A., Grigorieff, N., Musacchio, A., and Nogales, E. (2010). The Ndc80 kinetochore complex forms oligomeric arrays along microtubules. Nature *467*, 805–810.

Alushin, G.M., Musinipally, V., Matson, D., Tooley, J., Stukenberg, P.T., and Nogales, E. (2012). Multimodal microtubule binding by the Ndc80 kinetochore complex. Nat. Struct. Mol. Biol. *19*, 1161–1167.

Canman, J.C., Cameron, L.A., Maddox, P.S., Straight, A., Tirnauer, J.S., Mitchison, T.J., Fang, G., Kapoor, T.M., and Salmon, E.D. (2003). Determining the position of the cell division plane. Nature *424*, 1074–1078.

Carmena, M., Wheelock, M., Funabiki, H., and Earnshaw, W.C. (2012). The chromosomal passenger complex (CPC): from easy rider to the godfather of mitosis. Nat. Rev. Mol. Cell Biol. *13*, 789–803.

Ciferri, C., Pasqualato, S., Screpanti, E., Varetti, G., Santaguida, S., Dos Reis, G., Maiolica, A., Polka, J., De Luca, J.G., De Wulf, P., et al. (2008). Implications for kinetochore-microtubule attachment from the structure of an engineered Ndc80 complex. Cell *133*, 427–439.

Cooke, C.A., Heck, M.M., and Earnshaw, W.C. (1987). The inner centromere protein (INCENP) antigens: movement from inner centromere to midbody during mitosis. J. Cell Biol. *105*, 2053–2067.

DeLuca, J.G., Gall, W.E., Ciferri, C., Cimini, D., Musacchio, A., and Salmon, E.D. (2006). Kinetochore microtubule dynamics and attachment stability are regulated by Hec1. Cell *127*, 969–982.

Earnshaw, W.C., and Cooke, C.A. (1991). Analysis of the distribution of the INCENPs throughout mitosis reveals the existence of a pathway of structural changes in the chromosomes during metaphase and early events in cleavage furrow formation. J. Cell Sci. *98*, 443–461.

Goto, H., Kiyono, T., Tomono, Y., Kawajiri, A., Urano, T., Furukawa, K., Nigg, E.A., and Inagaki, M. (2006). Complex formation of Plk1 and INCENP required for metaphase-anaphase transition. Nat. Cell Biol. *8*, 180–187.

Gruneberg, U., Neef, R., Honda, R., Nigg, E.A., and Barr, F.A. (2004). Relocation of Aurora B from centromeres to the central spindle at the metaphase to anaphase transition requires MKlp2. J. Cell Biol. *166*, 167–172.

Guimaraes, G.J., Dong, Y., McEwen, B.F., and Deluca, J.G. (2008). Kinetochore-microtubule attachment relies on the disordered N-terminal tail domain of Hec1. Curr. Biol. *18*, 1778–1784.

Hill, E., Clarke, M., and Barr, F.A. (2000). The Rab6-binding kinesin, Rab6-KIFL, is required for cytokinesis. EMBO J. *19*, 5711–5719.

Hümmer, S., and Mayer, T.U. (2009). Cdk1 negatively regulates midzone localization of the mitotic kinesin Mklp2 and the chromosomal passenger complex. Curr. Biol. *19*, 607–612.

Hutterer, A., Glotzer, M., and Mishima, M. (2009). Clustering of centralspindlin is essential for its accumulation to the central spindle and the midbody. Curr. Biol. *19*, 2043–2049.

Kitagawa, M., Fung, S.Y.S., Onishi, N., Saya, H., and Lee, S.H. (2013). Targeting Aurora B to the equatorial cortex by MKlp2 is required for cytokinesis. PLoS ONE *8*, e64826.

Lee, S.H., McCormick, F., and Saya, H. (2010). Mad2 inhibits the mitotic kinesin MKlp2. J. Cell Biol. *191*, 1069–1077.

Meunier, S., and Vernos, I. (2012). Microtubule assembly during mitosis - from distinct origins to distinct functions? J. Cell Sci. *125*, 2805–2814.

Miller, S.A., Johnson, M.L., and Stukenberg, P.T. (2008). Kinetochore attachments require an interaction between unstructured tails on microtubules and Ndc80(Hec1). Curr. Biol. *18*, 1785–1791.

Mirchenko, L., and Uhlmann, F. (2010). Sli15(INCENP) dephosphorylation prevents mitotic checkpoint reengagement due to loss of tension at anaphase onset. Curr. Biol. *20*, 1396–1401.

Mishima, M., Kaitna, S., and Glotzer, M. (2002). Central spindle assembly and cytokinesis require a kinesin-like protein/RhoGAP complex with microtubule bundling activity. Dev. Cell *2*, 41–54.

Mishima, M., Pavicic, V., Grüneberg, U., Nigg, E.A., and Glotzer, M. (2004). Cell cycle regulation of central spindle assembly. Nature *430*, 908–913.

Nakajima, Y., Cormier, A., Tyers, R.G., Pigula, A., Peng, Y., Drubin, D.G., and Barnes, G. (2011). Ipl1/Aurora-dependent phosphorylation of Sli15/INCENP regulates CPC-spindle interaction to ensure proper microtubule dynamics. J. Cell Biol. *194*, 137–153.

Neef, R., Preisinger, C., Sutcliffe, J., Kopajtich, R., Nigg, E.A., Mayer, T.U., and Barr, F.A. (2003). Phosphorylation of mitotic kinesin-like protein 2 by polo-like kinase 1 is required for cytokinesis. J. Cell Biol. *162*, 863–875.

Pereira, G., and Schiebel, E. (2003). Separase regulates INCENP-Aurora B anaphase spindle function through Cdc14. Science *302*, 2120–2124.

Rhind, N., and Russell, P. (2012). Signaling pathways that regulate cell division. Cold Spring Harb. Perspect. Biol. *4*, a005942.

Subramanian, R., Wilson-Kubalek, E.M., Arthur, C.P., Bick, M.J., Campbell, E.A., Darst, S.A., Milligan, R.A., and Kapoor, T.M. (2010). Insights into antiparallel microtubule crosslinking by PRC1, a conserved nonmotor microtubule binding protein. Cell *142*, 433–443.

Verhey, K.J., and Hammond, J.W. (2009). Traffic control: regulation of kinesin motors. Nat. Rev. Mol. Cell Biol. *10*, 765–777.

Wei, R.R., Al-Bassam, J., and Harrison, S.C. (2007). The Ndc80/HEC1 complex is a contact point for kinetochore-microtubule attachment. Nat. Struct. Mol. Biol. *14*, 54–59.

Zhu, C., Lau, E., Schwarzenbacher, R., Bossy-Wetzel, E., and Jiang, W. (2006). Spatiotemporal control of spindle midzone formation by PRC1 in human cells. Proc. Natl. Acad. Sci. USA *103*, 6196–6201.